International Journal of Multiphase Flow 106 (2018) 280–295

Contents lists available at ScienceDirect

International Journal of Multiphase Flow

journal homepage: www.elsevier.com/locate/ijmulflow

Spray formation and atomization characteristics of non-Newtonian impinging jets at high Carreau numbers

Neil S. Rodrigues*, Varun Kulkarni, Jian Gao, Jun Chen, Paul E. Sojka*

M.J. Zucrow Laboratories, Purdue University, West Lafayette, IN 47907, USA

ARTICLE INFO

Article history:
Received 4 February 2018
Revised 11 May 2018
Accepted 22 May 2018
Available online 26 May 2018

Keywords:
Non-Newtonian sprays
Phase doppler anemometry
Impinging jets

ABSTRACT

Over the last two decades there has been a renewed interest in employing shear-thinning non-Newtonian liquids for use with liquid rocket engines due to a desire for greater safety and performance. Since the difficulty with producing quality atomization is the main disadvantage for using non-Newtonian liquid propellants, further understanding of the breakup physics and accurate measurement of the spray characteristics is needed. The atomization produced by the like-on-like jet impingement of three different non-Newtonian liquids was experimentally investigated in this work using shadowgraphy and Phase Doppler Anemometry (PDA) at high strain rates (10^5–10^6), which correspond closely to the strain rates used in practical rocket engines. The three water-based solutions tested were of two different grades of Carboxymethylcellulose (CMC): 0.5 wt.-% CMC-7HF, 0.8 wt.-% CMC-7MF, and 1.4 wt.-% CMC-7MF. The Bird–Carreau rheological model was used to characterize the non-Newtonian behavior and a generalized Carreau number was used as the primary parameter to characterize the liquid viscosity inside the orifice at injection. A generalized Bird–Carreau jet Reynolds number $Re_{j,gen\text{-}BC}$ and the jet Weber number We_j were used as primary parameters to characterize the spray formation, sheet breakup length, drop size, and drop velocity. The unique spray formation a behavior of the three non-Newtonian liquids was ascribed to the relative influence of the inertial vs. viscous forces, primarily expressed through $Re_{j,gen\text{-}BC}$. At many relatively high inertial force test conditions, drops in the spray were near spherical and could be reliably measured using PDA. Spray characteristics of intact sheet length, drop diameter, and drop velocity were observed to be strong functions of $Re_{j,gen\text{-}BC}$. In addition to providing fundamental understanding to aid with injector design for liquid rocket engine applications using non-Newtonian liquids, the measurements presented in this work could be used to validate a future closed-form analytical non-Newtonian atomization model, which remains an open problem in non-Newtonian impinging jets literature.

1. Introduction

In recent years, liquid rocket propulsion systems have emerged as the most popular form of propulsion for space exploration and defense operations. Reasons for the popularity of liquid rocket systems include controllability through throttling and higher specific impulse compared to other forms of chemical combustion. However, one major disadvantage of liquid propellants is the hazards associated with potential propellant leakage (Humble et al., 1992). Due to the very high level of toxicity of some liquid propellants, increasing safety is an important area of need (Palaszewski, 1994). As a result, there has been a renewed interest in using impinging jets with non-Newtonian liquids as propellants over the past two decades as a means of overcoming the disadvantages of liquid propellants. Recent studies in this area include: Chojnacki and Feikema (1997), Fakhri and et al. (2010), Baek and et al. (2011), Yang et al., (2012), Negri and et al. (2013), Mallory and Sojka (2014a and 2014b), Ma et al., (2015), and Xiao et al., (2015). Among existing literature of non-Newtonian impinging jets, there is a particular scarcity of studies that use Phase Doppler Anemometry (PDA) to characterize the drop size and drop velocity.

Newtonian liquids have a constant value for viscosity regardless of strain rate, whereas the viscosity of non-Newtonian liquids varies with strain rate. The ability of shear-thinning non-Newtonian liquids to only flow easily when under pressure is desirable for propellant resupply, because containment and cleanup could be more manageable in the event of an accident. While on a mission, the risks from a damaged fuel or oxidizer tank could also be mitigated by using highly viscous non-Newtonian liquids (Nathan and Rahimi, 2002). One main disadvantage of using non-Newtonian liquids, however, is the difficulty in their atomization. This is because viscosity inhibits breakup (Lefebvre, 1989). Strong

* Corresponding authors.
E-mail addresses: neilrodrigues@asme.org (N.S. Rodrigues), sojka@ecn.purdue.edu (P.E. Sojka).

https://doi.org/10.1016/j.ijmultiphaseflow.2018.05.017
0301-9322/

shear-thinning behavior is therefore a requirement for the non-Newtonian liquid. Shear-thinning behavior is the tendency of certain liquids to decrease in viscosity when under increased strain rates (Morrison, 2001).

Inelastic liquids were considered in this work, rather than gelled or viscoelastic liquid solutions, in order to study the effects of the shear-thinning behavior on the atomization characteristics without introducing elastic or yield stress effects. Fluid flow behavior for shear-thinning, inelastic, non-Newtonian liquids that do not show a yield stress can be best characterized using the Bird–Carreau model (Carreau, 1972). The Bird–Carreau model is a simplification of the Carreau–Yasuda model, where the parameter a, which is the shape of the transition region between the rapidly decreasing part of the viscosity curve and the zero-strain rate plateau, is set to the value of 2 for shear-thinning liquids. The expression for the Bird–Carreau rheological model is:

$$\eta(\dot{\gamma})_{BC} = [1 + Cu^2]^{\frac{n-1}{2}}(\eta_0 - \eta_\infty) + \eta_\infty, \tag{1}$$

$$Cu = \lambda\dot{\gamma}. \tag{2}$$

In Eq. (1) η is the effective viscosity based on the Bird–Carreau model as a function of the strain rate $\dot{\gamma}$. Zero- and infinite-strain rate viscosity limits are symbolized by η_0 and η_∞ respectively. The parameter n is called the flow behavior index and describes the rapidly decreasing part of the viscosity curve (Morrison, 2001). The Carreau number Cu is defined in Eq. (2) as the parameter λ (which describes the characteristic time at which shear-thinning begins) multiplied by the strain rate $\dot{\gamma}$ (Shenoy, 2013). The Carreau number is a dimensionless parameter that indicates if a given fluid at a particular strain-rate is in the shear-thinning region.

A common injector for liquid rocket engines is the impinging jet injector due to ease in fabrication, desirable atomization characteristics, and high-performance mixing (Humble et al., 1992). Using two jets of the same liquid (either fuel or oxidizer) with the impinging jet injector is called the like-on-like doublet configuration. The general primary atomization behavior of impinging jets involves two jets colliding at an oblique angle to form a flat liquid sheet that is perpendicular to the momentum vectors of the two jets. Instabilities on the sheet promote sheet breakup into ligaments, which then experience further breakup into drops (Heidmann et al., 1957). The drop size and drop velocity depend on sheet parameters such as sheet thickness and sheet velocity, which in turn depend on jet parameters such as jet velocity, jet diameter, and the impingement angle between the two jets 2θ. The aerodynamic and inertial forces promote fragmentation of the liquid sheet, the surface tension force opposes breakup, and the viscous force serves to delay breakup (Lefebvre, 1989). Fig. 1 shows the general breakup process using a shadowgraph of a deionized (DI) water spray.

The dimensionless parameters used to study impinging jet atomization are the jet Reynolds number (inertial force to viscous force) and the jet Weber number (inertial force to surface tension force). Due to the strain rate dependency of viscosity, the Reynolds number must be modified for non-Newtonian liquids. Mallory and Sojka (2014a,2014b) provide a generalized Bird–Carreau jet Reynolds number $Re_{\text{j,gen-BC}}$, which is used in this work as the primary dimensionless parameter to characterize the spray characteristics. The generalized Bird–Carreau jet Reynolds number is the ratio of the inertial force to the shear-thinning viscous force. This expression for $Re_{\text{j,gen-BC}}$ has been recast here to:

$$\text{Re}_{j,gen-BC} = \frac{\rho_L U_j d_j}{\eta_{j,gen-BC}}, \tag{3}$$

$$\eta_{j,gen-BC} = ((1 + Cu_{j,gen}{}^2)^{\frac{n-1}{2}}(\eta_0 - \eta_\infty) + \eta_\infty)\left(\frac{3n+1}{4n}\right), \tag{4}$$

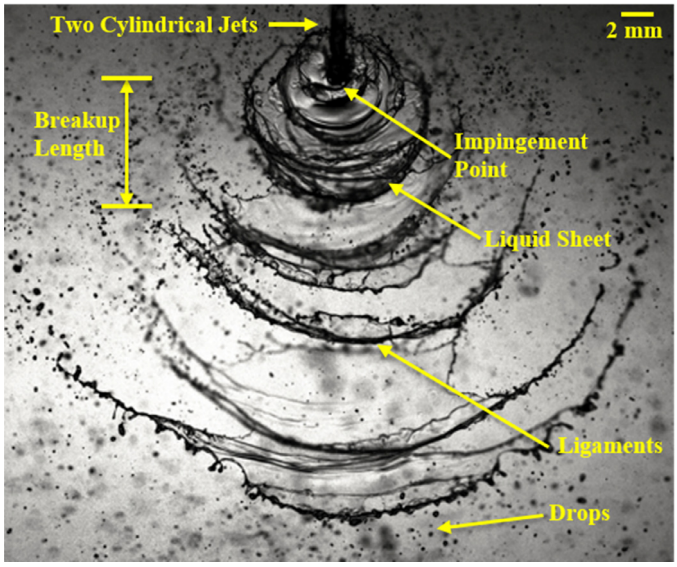

Fig. 1. Shadowgraph of DI water spray highlighting the impinging jet atomization process.

$$Cu_{j,gen} = \frac{3n+1}{4n}\frac{8U_j}{d_j}\lambda. \tag{5}$$

The terms in Eq. (3) are the liquid density ρ_L, jet velocity U_j, jet diameter d_j, and effective viscosity of the liquid jet based on the Bird–Carreau model $\eta_{\text{j,gen-BC}}$. The expression for the effective viscosity is provided in Eq. (4) and depends of the Bird–Carreau parameters and the jet Carreau number Cu_j. The generalized jet Carreau number is defined in Eq. (5) using the Bird–Carreau parameters, jet diameter, and jet velocity.

For the case of a Newtonian liquid: η_0 and η_∞ are both equal to the Newtonian dynamic viscosity μ_L and the flow behavior index $n = 1$. Under these conditions, the generalized Bird–Carreau jet Reynolds numbers reverts back to the Newtonian jet Reynolds number:

$$\text{Re}_j = \frac{\rho_L U_j d_j}{\mu_L}. \tag{6}$$

The jet Weber number We_j is another important parameter, particularly for studies using low viscosity liquids. The expression for the jet Weber number is:

$$We_j = \frac{\rho_L U_j{}^2 d_j}{\sigma}. \tag{7}$$

In the above expression, σ is the liquid-air surface tension.

The spray characterization of drop size and drop velocity is important for combustion purposes because of their influence on mass transfer and mass dispersal. The arithmetic mean diameter (D_{10}), Sauter mean diameter (D_{32}), and mass median diameter (MMD) are typically used as representative diameters to characterize drop size for impinging jet sprays. D_{10} is used widely for comparison and D_{32} represents the volume to surface area ratio. MMD is a representative diameter such that 50% of total liquid volume is in drops of smaller diameters. Information on calculating D_{10}, D_{32}, and MMD is widely available in references such as Lefebvre (1989). For combustion purposes, such as impinging jet atomization for liquid rocket engines, D_{32} is considered by many to be the most applicable mean diameter because it best describes the fineness of the spray. Although the representative diameters provide a convenient means to represent variation with operating conditions and dimensionless parameters such as the Reynolds and Weber numbers, they do not adequately reveal features of the atomization

process such as spread and skewness of the drop size distribution. Probability density functions (pdfs), on the other hand, are exact representations of the range of drop sizes produced by a spray and can therefore reveal these features. Number, surface area, and volume pdfs are used in this work to characterize the polydisperse nature of the spray. The number pdf f_0 is the probability density that a drop has diameter D, the surface area pdf f_2 is the probability density that a drop has surface area πD^2, and the volume pdf is the probability density that a drop has a volume $\pi D^3/6$. Information on calculating the pdfs are also widely available in references such as Lefebvre (1989).

Spray characterization of jet impingement with Newtonian liquids has been studied extensively in existing literature, starting with Heidmann et al. (1957). Four distinct spray regimes were identified, which evolve with the jet Reynolds number: *closed rim with drop formation* ($Re_j < 2500$), *periodic drop* ($2500 < Re_j < 5000$), *open rim* ($5000 < Re_j < 10{,}000$), and *fully developed* ($10{,}000 < Re_j$). The jet Reynolds number was observed to have a great effect on the flavor of the breakup process. For instance, in the *closed rim* regime, a distinct sheet was formed and drops were shed from the rim of the sheet. In contrast, for the *fully developed* regime the sheet was actually no longer clearly visible; ligaments and drops were observed to directly emit from near the impingement point. However, distinct boundaries for the spray patterns based on Re_j have not been well defined due to the influence of other relevant impinging jet parameters such as the angle of impingement 2θ. Impinging jet atomization studies with Newtonian liquids over the last two decades include: Ibrahim and Przekwas (1991), Ryan et al., (1995), and Li and Ashgriz (2006).

Recently, Rodrigues et al. (2015) more accurately characterized the drop size and drop velocity of DI water impinging jets sprays using Phase Doppler Anemometry (PDA). Developments in PDA technology enabled the measurement of the smallest drops in the spray compared to previous works such as that of Ryan et al. (1995). The jet Weber number was used to characterize the D_{10}, D_{32}, and *MMD* drop diameters and the mean axial drop velocity $U_{z\text{-mean}}$. Number, surface area, and volume pdfs were used to characterize the polydisperse nature of the spray. Rodrigues and coworkers also provided an analytical expression to predict drop diameter depending on the assumed jet velocity profile inside the orifice: uniform, parabolic, or turbulent.

Although the atomization behavior of non-Newtonian liquids has been studied in recent years, there is still a very incomplete understanding regarding the variety of effects that non-Newtonian behavior has on atomization. Furthermore, as noted by Von Kampen et al. (2006), atomization regimes for non-Newtonian liquids have not been well defined. The available literature indicates an inverse relationship between the jet Reynolds number and atomization characteristics such as sheet breakup length (Baek et al., 2011; Mallory and Sojka, 2014a,2014b). The majority of non-Newtonian impinging jet studies in literature that report drop size use either image analysis from shadowgraphs (Yang et al., 2012; Negri et al., 2013; Mallory and Sojka, 2014a,2014b) or laser diffraction instrumentation (Fakhri et al., 2010; Baek et al., 2011). The recent study by Ma et al., (2015) is the only known study in literature that measures the drop size and drop velocity of a non-Newtonian impinging jet spray using PDA. This study reports the spatially resolved spray characteristics of two Carbopol solutions at several operating conditions.

Chojnacki and Feikema (1997) and Mallory and Sojka (2014a, 2014b) have presented some experimental measurements using water-based solutions of carboxymethylcellulose (CMC). The spray formation and characteristics in these studies were investigated using shadowgraphy for a relatively narrow set of test conditions and these earlier works do not provide drop size information using a high-fidelity technique such as PDA. This present work seeks to expand understanding of the spray formation and drop size of non-Newtonian liquids through further study of CMC solutions. The following is presented in this work: (i) Shadowgraphs of the impinging jet spray formation for a wide range of $Re_{j,gen\text{-}BC}$, (ii) sheet breakup length measurements from shadowgraphs, and (iii) mean values and distribution for drop size and drop velocity using PDA. This work is believed to be the first non-Newtonian impinging jets study to use PDA to characterize the drop size and drop velocity as a function of dimensionless parameters and is the only study outside of Ma et al. (2015) that uses PDA to study non-Newtonian impinging jet sprays.

2. Experimental setup

Since the processes of injection, atomization, mixing, and combustion occur nearly simultaneously in a liquid rocket engine, uncoupling of the various processes is required for detailed analysis (Humble et al., 1992). To eliminate the combustion process, water has been traditionally used instead of the propellant for liquid impinging jet atomization studies. For non-Newtonian atomization studies, water with a non-Newtonian agent is typically used to study the spray characteristics. Two different grades of carboxymethylcellulose (CMC) were used in this investigation – high molecular weight CMC-7HF (700 kDa) and medium molecular weight CMC-7MF (250 kDa). The mass fraction was used to quantify the amount of agent added into the water to formulate the solution. A total of three different CMC solutions were used for this work: 0.5 wt.-% CMC-7HF, 0.8 wt.-% CMC-7MF, and 1.4 wt.-% CMC-7MF. Deionized water was also used as a reference liquid. The three CMC liquid solutions were mixed at room temperature using a steel bowl and a low shear mixer. Special care was taken during the mixing process and the solutions were left to stir until they were determined to be homogenous by visual inspection. The three CMC solutions can be described as homogenous, soluble, and highly viscous liquids.

2.1. Bulk and interfacial rheologies

A rotational rheometer was used to determine the bulk rheological properties at low strain rates (10^{-1} to 10^2 1/s). The cone-and-plate configuration (60 mm, 2.025° angle) was used for all measurements in controlled-rate mode. Controlled-torque strain rates were enacted on the samples using magnetic thrust bearing technology and the resulting stresses were measured. A sweep up test was conducted with increasing strain rates. Sweeping the strain rates from lowest to highest values preserves the solution structure during testing. In order to determine if any thixotropic behavior was present, a sweep down test was also conducted. A capillary rheometer was used to determine the viscosity of the investigated solutions at high strain rates (10^3 to 10^5 1/s). A 0.606 mm capillary die was used for all capillary rheometer measurements. The pressure drop was recorded once the flow became fully developed and was used to determine the viscosity. The Weissenberg–Rabinowitsh correction factor as outlined in Morrison (2001) was used for all measurements. A 5% tolerance was set for all viscosity measurements and criterion for a data point to be considered valid was three consecutive measurements within the tolerance.

Non-Newtonian behavior was observed for all investigated solutions, as indicated by the shear stress versus strain rate behavior in Fig. 2. A yield stress was not observed for the three CMC solutions investigated, permitting the use of a non-Newtonian model that does not have a term for yield stress, such as the Bird–Carreau model. The 0.5 wt.-% CMC-7HF solution was observed to show stronger shear-thinning behavior compared to the two CMC-7MF solutions at 0.8 wt.-% and 1.4 wt.-%. This is believed to be due to the higher molecular weight of CMC-7HF (700 kDa) compared

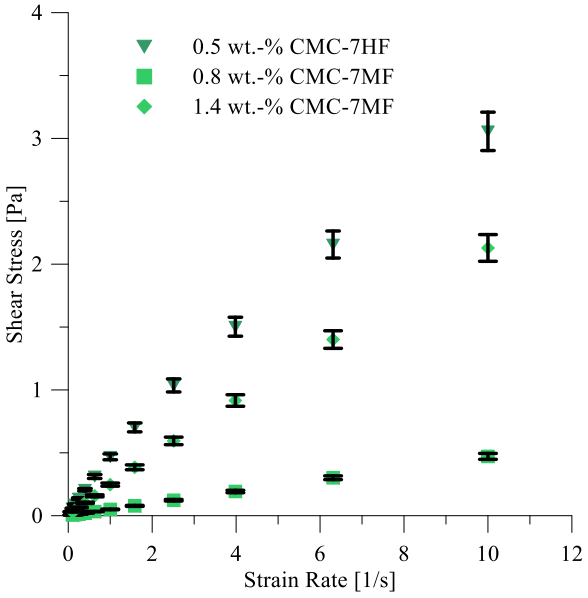

Fig. 2. Shear stress vs. strain rate for three CMC liquids investigated.

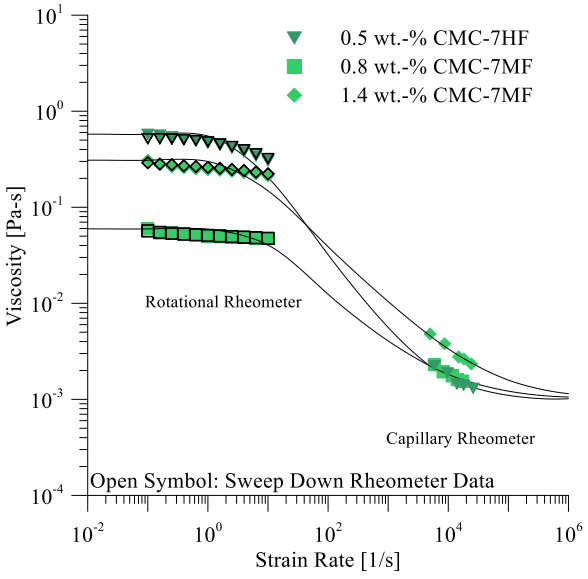

Fig. 3. Viscosity vs. strain rate for the three CMC liquids investigated.

to that of CMC-7MF (200 kDa). Due to its higher polymer concentration, the 1.4 wt.-% CMC-7MF solution was observed to show stronger shear-thinning behavior compared to the 0.8 wt.-% CMC-7MF solution. Mallory and Sojka (2014a,2014b) had previously considered the storage and loss moduli of these three CMC solutions and concluded that they behave as inelastic liquids.

Fig. 3 presents the viscosity vs. strain rate behavior for the three CMC solutions using the rotational and capillary rheometer measurements and the Bird–Carreau curve. A Newtonian plateau at very low strain rates and shear-thinning behavior with increasing strain rates was experimentally observed for all three liquids. However, a second Newtonian plateau at high strain rates was not experimentally observed. Following studies in literature such as Madlener and Ciezki (2012), it was assumed that the infinite-strain rate viscosity of the three non-Newtonian liquids was that of the base fluid (water). The literature value of 0.001 Pa-s was taken as the viscosity of water. This approach, however, is different from the one previously taken by Mallory and Sojka (2014a,2014b), and as

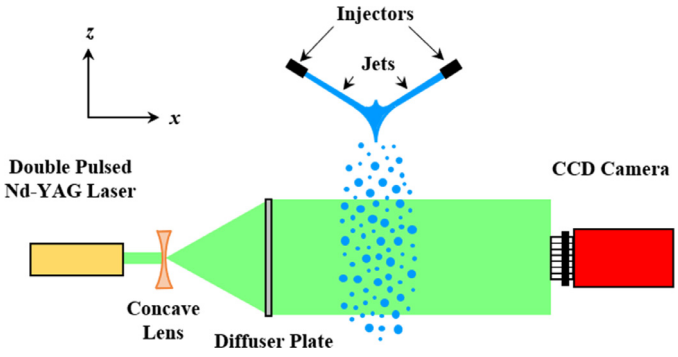

Fig. 4. Schematic of the shadowgraphy set-up.

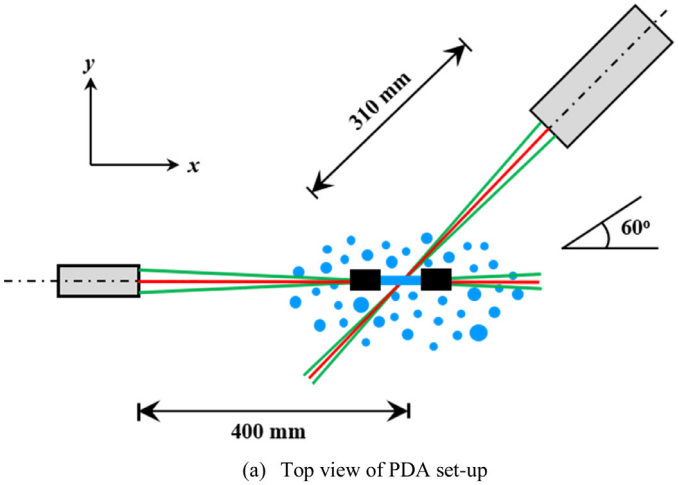

(a) Top view of PDA set-up

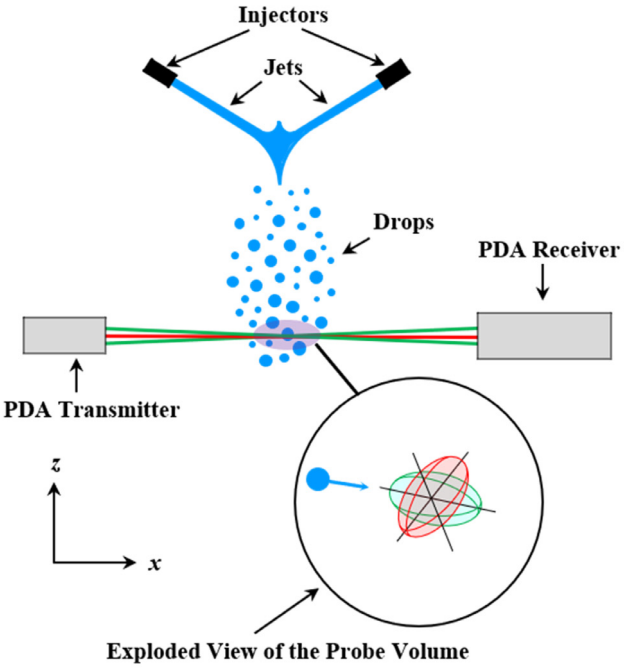

(b) Side view of PDA set-up

Fig. 5. Schematic of the PDA set-up.

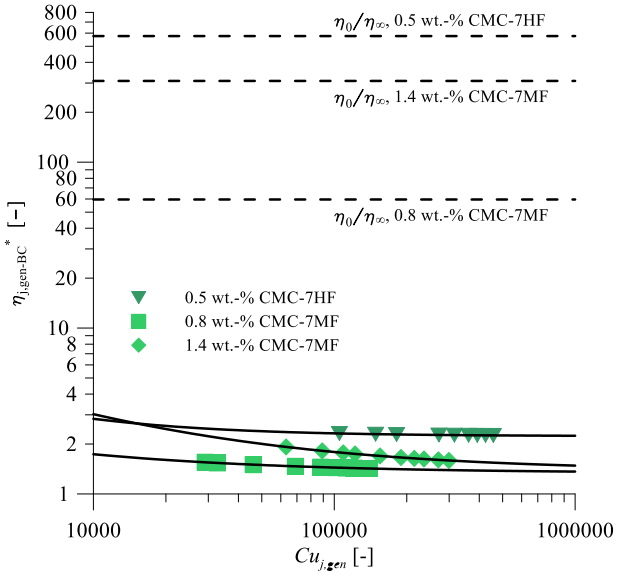

Fig. 6. Dimensionless generalized BC jet viscosity $\eta_{j,gen\text{-}BC}^*$ vs. generalized Jet Carreau number $Cu_{j,gen}$.

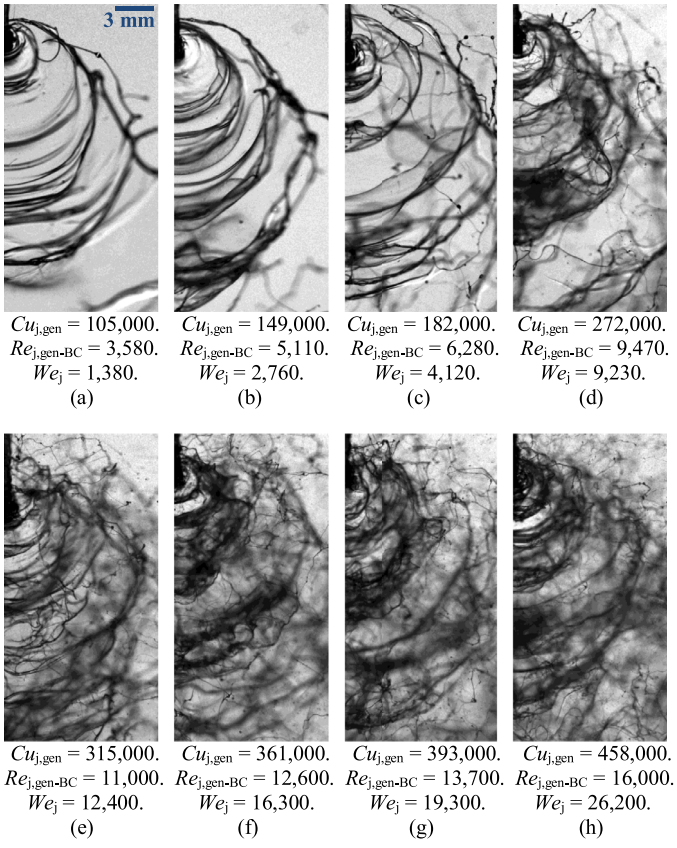

Fig. 7. Spray formation of 0.5 wt.-% CMC-7HF with increasing $Cu_{j,gen}$, $Re_{j,gen\text{-}BC}$, and We_j.

a result dissimilar but more accurate Bird–Carreau parameters are presented in this work. The Bird–Carreau parameters used in this work for all three CMC solutions are presented in Table 1. Based on Fig. 3, it can be noted that no significant thixotropic behavior was observed from sweep up and sweep down tests.

A du Noüy ring tensiometer was used to measure the liquid-air surface tension of the three solutions. The surface tension was

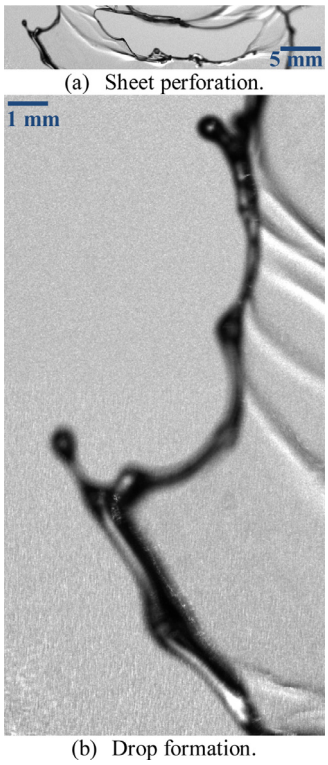

Fig. 8. Sheet perforation and drop formation for 0.5 wt.-% CMC-7HF at $Cu_{j,gen}$ = 105,000, $Re_{j,gen\text{-}BC}$ = 3580, and We_j = 1380.

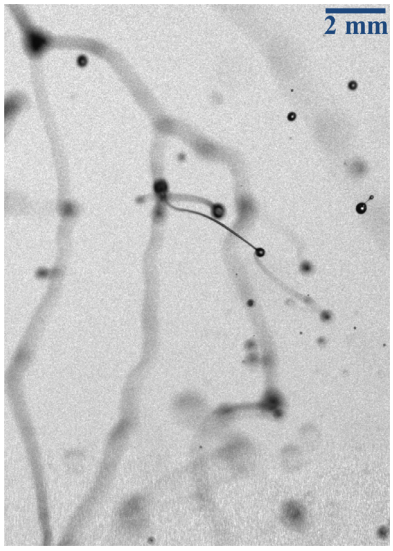

Fig. 9. Drop formation for 0.5 wt.-% CMC-7HF at $Cu_{j,gen}$ = 149,000, $Re_{j,gen\text{-}BC}$ = 5110, and We_j = 2760.

Table 1
Bird-Carreau rheological parameters for the three CMC liquids investigated.

Parameter	0.5 wt.-% CMC-7HF	0.8 wt.-% CMC-7MF	1.4 wt.-% CMC-7MF
η_0 [Pa-s]	0.576 ± 0.029	0.0596 ± 0.0030	0.309 ± 0.015
η_∞ [Pa-s]	0.001	0.001	0.001
n [-]	0.169 ± 0.008	0.427 ± 0.021	0.397 ± 0.020
λ [s]	0.334 ± 0.017	0.173 ± 0.009	0.324 ± 0.016

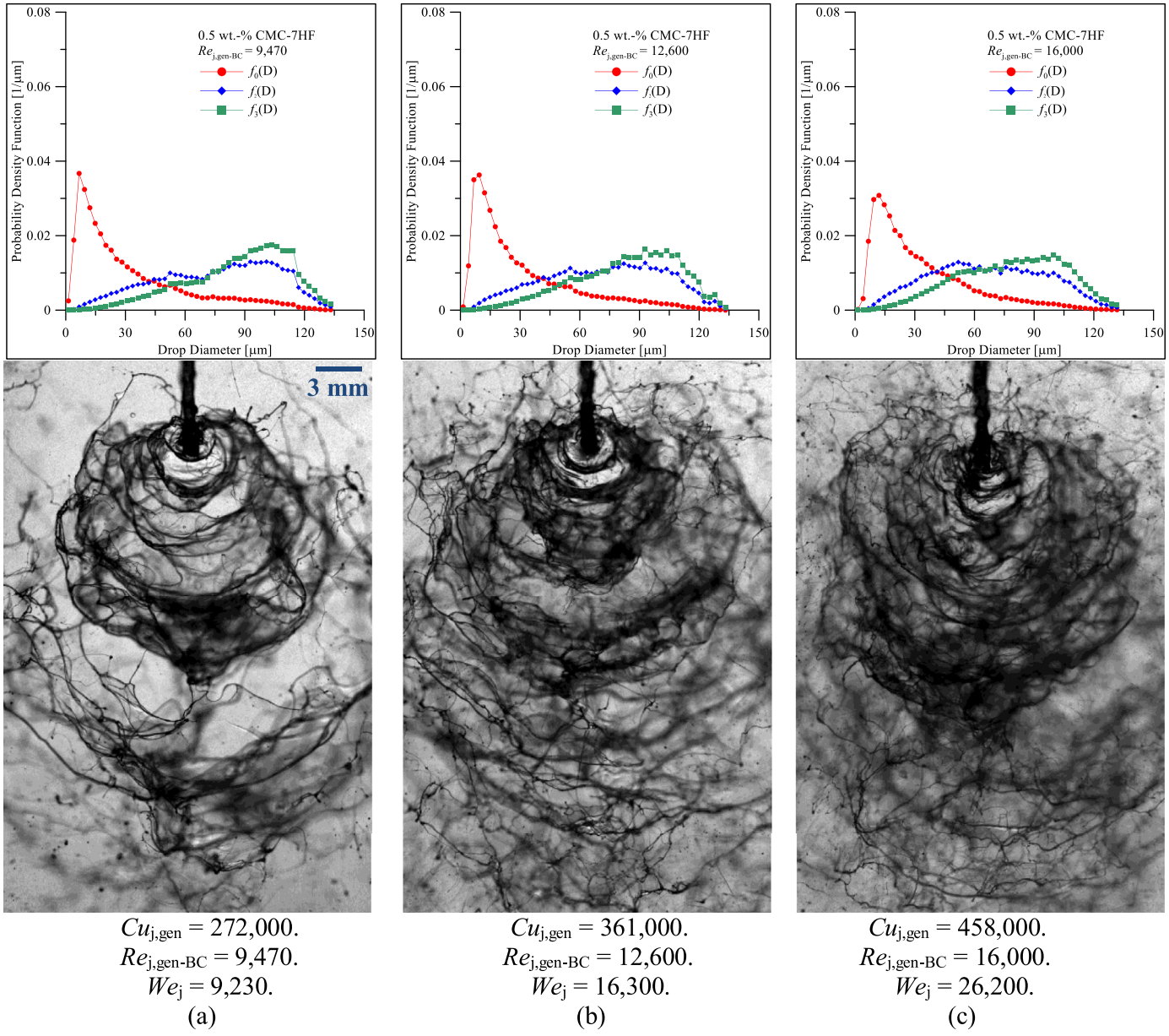

Fig. 10. Number, surface area, and volume pdfs versus drop diameters with corresponding spray patterns for select 0.5 wt.-% CMC-7HF sprays with increasing $Cu_{j,gen}$, $Re_{j,gen-BC}$, and We_j.

determined by relating the measured force required to raise the ring to the liquid-air surface tension. The ring and dish were rinsed with deionized water and cleaned using isopropyl alcohol between tests, and any impurities left on the ring were burned away using a propane torch. Ten independent measurements were taken for each liquid, and one standard deviation was used as the measurement uncertainty. A correction factor was applied to account for the ring geometry and liquid properties based on the work of Zuidema and Waters (1941).

It was discovered that all three CMC solutions considered in this work have liquid-air surface tension values very close to the literature reported value of water (0.0728 N/m), as presented in Table 2. Therefore, the liquid-air surface tensions of 0.5 wt.-% CMC-7HF, 0.8 wt.-% CMC-7MF, and 1.4 wt.-% CMC-7MF were taken to be that of the literature value of water for jet Weber number calculation purposes. The liquid-air surface tension of water was also measured using the tensiometer for reference and was observed to be 0.0727 ± 0.0003 N/m.

Table 2
Experimentally measured values of liquid-air surface tension for the three CMC liquids investigated.

	0.5 wt.-% CMC-7HF	0.8 wt.-% CMC-7MF	1.4 wt.-% CMC-7MF
σ [N/m]	0.0727 ± 0.0002	0.0724 ± 0.0005	0.0728 ± 0.0001

2.2. Spray facility and diagnostics

The custom designed experimental apparatus used to create atomization in this study is essentially identical to the facility used by Rodrigues et al. (2015). Rotational stages and translation stages were used to specify the impingement angle at $2\theta = 100°$ and the free jet length-to-orifice diameter ratio at $x/d_0 = 60$. Both the internal length-to-orifice diameter ratio $L/d_0 = 20$ and the orifice diameter $d_0 = 0.686$ mm were specified using designated tip elements. The ambient gas was air at atmospheric temperature and pressure

Table 3
Range of dimensionless numbers used in present work for the three CMC liquids investigated.

	0.5 wt.-% CMC-7HF	0.8 wt.-% CMC-7MF	1.4 wt.-% CMC-7MF
$Re_{j,gen\text{-}BC}$ x 10^3	3.58–16.0	4.77–25.0	4.32–24.7
We_j x 10^3	1.38–26.2	1.10–25.3	1.38–31.0

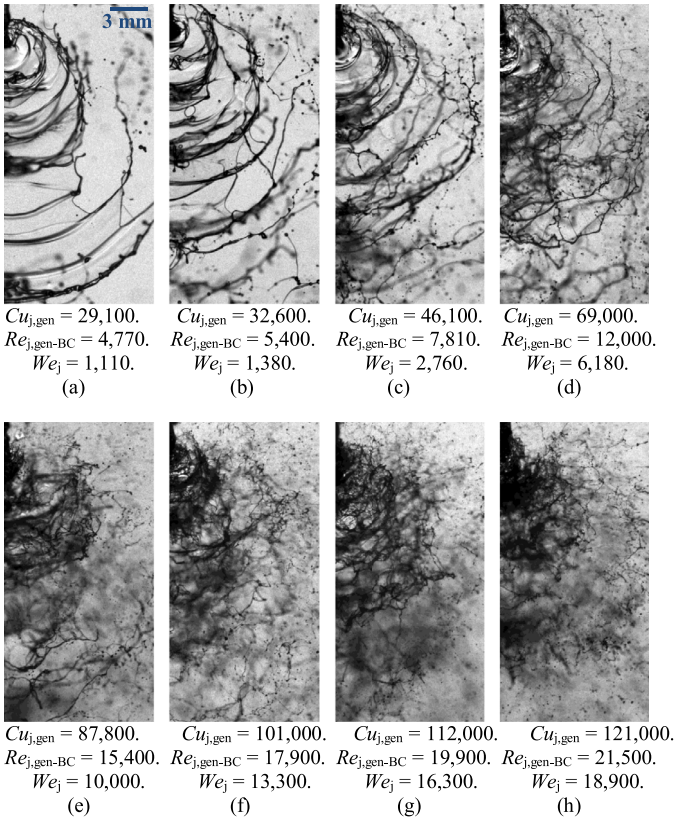

Fig. 11. Spray formation of 0.8 wt.-% CMC-7MF with increasing $Cu_{j,gen}$, $Re_{j,gen\text{-}BC}$, and We_j.

and the literature value $\rho_g = 1.2\,kg/m^3$ was used for gas density of the air. $1000\,kg/m^3$ was used as the density for the liquid solutions ρ_L. The mean jet velocity $\bar{U}_j$ was determined based on mass flow rate calculations from collecting liquid in a vessel for test durations of 30 seconds and measuring the mass of the collected liquid using a balance. This was repeated three times to ensure statistically significant values. A discharge coefficient of 0.70 ± 0.02 was measured for the orifices. Despite the high mean jet velocities, cavitation was not visibly observed for the test conditions used in this work. This can be attributed to the fairly high L/d_0 ratio, the rather small orifice diameter, and the non-Newtonian behavior of the CMC solutions.

The operating pressure was varied for the liquids tested in order to control $Re_{j,gen\text{-}BC}$ and We_j through the mean jet velocity. The range of $Re_{j,gen\text{-}BC}$ and We_j for this work, calculated based on the bulk and interfacial rheological measurements, are presented in Table 3. The rather high generalized Bird–Carreau jet Reynolds numbers and jet Weber numbers indicate that inertia dominates over the viscous and capillary forces respectively for the test conditions considered. The Kline–McClintock approach (Kline and McClintock, 1953) was used to calculate the percent uncertainty for the generalized Bird–Carreau jet Reynolds number and the jet Weber number.

The experimental setup for imaging the impinging jets is shown in Fig. 4. A double-pulsed Nd: YAG laser beam with a pulse width of 6 ns (short enough to freeze the motion of the liquid) was used to provide the back illumination. In order to reduce coherence, the laser beam was first expanded and then projected to a diffuser. No interference patterns were observed and the effect of the speckle noise on image quality was unnoticeable. The light produced by the diffuser provided back-illumination for the CCD camera, which was focused on the plane of the two impinging jets. The sheet breakup length was extracted from the shadowgraphs. Ten independent breakup length measurements were collected for each test condition and one standard deviation was used as the measurement uncertainty.

Measurements of drop size and drop velocity were obtained using a Phase Doppler Anemometry (PDA) system. PDA measures the drop diameter by finding a phase difference between Doppler signals. The drop velocity was measured using laser Doppler anemometry (LDA), which measures the frequency of the Doppler bursts and correlates this signal to drop velocity. The PDA receiver was oriented 30° from the Nd: YAG laser beams produced by the PDA transmitter. The PDA transmitter was equipped with a 400 mm focal length lens and the PDA receiver was equipped with a 310 mm focal length lens. A schematic of the set-up for the PDA optical diagnostics is provided in Fig. 5(a) and the probe volume in Fig. 5(b) shows the ellipsoid of intersection of the four laser beams. The ellipsoid corresponds to fringes that move at the Bragg cell frequency of 40 MHz. When a particle enters this probe volume, its velocity is measured relative to these moving fringes based on the Doppler effect. The size is measured based on a phase difference generated by reflection/refraction of the laser light as it travels from the transmitter to the receiver, passing through the drop in the probe volume. The theory behind PDA has been established in existing literature such as Albrecht et al., (2003).

The PDA was configured in non-coincidence mode with specified values for hardware and software settings to yield high validation and high data rates. The injector pair was mounted on transverse stages to enable movement in all three spatial dimensions for alignment. All measurements were obtained 5 cm below the point of impingement and 50,000 data points were collected for each test. An air-knife was used to produce a curtain of air in front of the PDA receiver to prevent drops from some test conditions from landing on the lens. In order to ensure that the air did not affect the measured values, measurements were obtained with and without the air curtain at a baseline condition. The PDA optical configuration with the selected aperture plate enabled a drop size measurement range between approximately 2.3 μm and 116.2 µm. Further details on the aperture plate selection can be found in Rodrigues (2014).

Mean drop diameters (D_{10}, D_{32}, and MMD) and mean axial drop velocity ($U_{z\text{-}mean}$) uncertainties were investigated by taking 5 repeated measurements at a baseline operating condition. The coefficient of variation, the ratio of one standard deviation to the mean, was used as the uncertainty for the PDA measurements. Table 4 provides the percent uncertainty for this work. Further details on determining the PDA uncertainty are also provided in Rodrigues (2014).

Table 4
Experimental uncertainty for presented measurements.

Quantity	Uncertainty (%)
$Re_{j,gen\text{-}BC}$	6.4
We_j	4.5
D_{10}	5.9
D_{32}	1.0
MMD	0.9
$U_{z\text{-}mean}$	2.9

3. Results and discussion

Low liquid viscosity is desired during injection and for the three CMC liquids used in this work, their effective viscosity inside the orifice approaches the Newtonian plateau of the solvent viscosity at the high strain rates inside the orifice considered (10^5–10^6 s^{-1}). This strain rate range reflect those typical for liquid rocket injection (Humble et al., 1992). Fig. 6 presents the dimensionless generalized BC jet viscosity $\eta_{j,gen\text{-}BC}{}^*$ vs. the generalized jet Carreau number $Cu_{j,gen}$ for the atomization conditions consider in this work. The generalized BC jet viscosity was made dimensionless using the viscosity of the solvent; DI water at room temperature ($\eta_\infty = 0.001$ Pa-s) was used as the solvent for this work. Fig. 6 shows that although the viscosity of the jet inside the orifice varies between 1.5 to 2.5 times that of water, the viscosity of each liquid solution remains relatively constant for the set of generalized jet Carreau numbers considered. In addition, the dimensionless zero-strain rate viscosity for each solution η_0 / η_∞ is shown in Fig. 6 to emphasize the difference between the apparent viscosity inside the orifice at the considered atomization conditions compared to their viscosity at very low strain rates ($<1 s^{-1}$).

3.1. Spray formation

Two impinging jets of 0.5 wt.-% CMC-7HF at $Cu_{j,gen} = 105{,}000$, $Re_{j,gen\text{-}BC} = 3{,}580$, and $We_j = 1{,}380$ were observed to form a liquid sheet bounded by a thick rim, as shown in Fig. 7(a). Instabilities were observed on the liquid sheet. However, sheet breakup was not observed due to the dominating viscous and surface tension forces. Rather, as seen in Fig. 8(a), sheet perforations further downstream of the impingement point were observed, Three-dimensional structures that can be described as wavy rims were observed on the regions of perforation. As presented in Fig. 8(b), the rim surrounding the sheet was observed to detach into string-like ligaments, which were then seen to breakup into a few drops. This atomization behavior was called the *perforated sheet* pattern.

Moderately increasing the inertial force for the 0.5 wt.-% CMC-7HF impinging jets resulted in spray patterns that contained tangled ligaments. Fig. 7(b) shows the *tangled web* pattern at $Cu_{j,gen} = 149{,}000$, $Re_{j,gen\text{-}BC} = 5110$, and $We_j = 2760$. Instabilities on the liquid sheet led to the formation of large three-dimensional structures that resemble a tangled web. Downstream from the impingement point, long string-like ligaments were observed to detach from the web. A few large drops were observed to form from the ligaments, as seen in Fig. 9. Further increasing the inertial forces to $Cu_{j,gen} = 182{,}000$, $Re_{j,gen\text{-}BC} = 6280$, and $We_j = 4120$ as shown in Fig. 7(c), resulted in changes to the morphology of the web. At these conditions it was somewhat difficult to determine where the liquid sheet experienced breakup and where the ligaments began to form. The structures inside the tangled web were observed to become increasingly dense with further increase in $Cu_{j,gen}$, $Re_{j,gen\text{-}BC}$, and We_j, as seen in Fig. 7(d) and (e).

Further increasing the inertial force led to the morphology of the sheet slowly changing from the *tangled web* pattern to one where instabilities caused the large liquid sheet to breakup and form an interconnecting web-like structure. This transition can be seen in Fig. 7(d) and (e) before becoming more apparent in Fig. 7(f)–(h). In this *ligament web* pattern, the web was observed to form long bow-like ligaments, which eventually form into drops further downstream. Since good drop formation were observed at these test conditions ($Cu_{j,gen} \geq 272{,}000$, $Re_{j,gen\text{-}BC} \geq 9470$, and $We_j \geq 9230$), Phase Doppler Anemometry (PDA) was used to measure the drop size at 5 cm below the impingement point at the centerline of the spray. Fig. 10(a) to (c) presents the far-field spray patterns and the corresponding number probability density function f_0, surface area probability density function f_2, and volume probability density function f_3 for three select conditions. The pdfs were created using a bin size of 50 and a sample size of 50,000 drops at each test condition. This observation of the number pdf not varying with an increase in the inertial force may be due to the larger number of small drops present in the spray at all three of the conditions within the range of high Cu_j, $Re_{j,gen\text{-}BC}$, and We_j considered. Rodrigues et al. (2015) had previously observed that the number pdf did not significantly vary for water sprays at high jet Weber numbers and had attributed this to the high quality of atomization at the conditions considered. On the other hand, Fig. 10 shows that variation was observed for the surface area and volume pdfs with increasing inertial force: surface area and volume pdfs showed a decrease in probability density for the relatively larger drops (>90 μm) and an increase in the probability density for the relatively mid-sized drops (60–90 μm). The surface area and volume pdfs, but not the number pdf, varying with increased inertial force was also observed by Rodrigues et al. (2015). Based on these observations, it can be concluded that at the high inertial force conditions considered for PDA measurements, additional inertial force does not increase the large number of small drops present in the spray but does decrease the number of relatively larger drops.

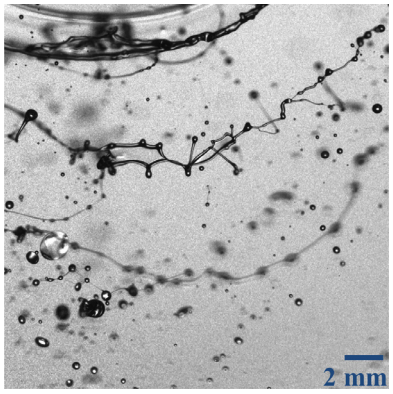

Fig. 12. Drop formation for 0.8 wt.-% CMC-7MF at $Cu_{j,gen} = 29{,}100$, $Re_{j,gen\text{-}BC} = 4770$, and $We_j = 1100$.

The spray formation of two impinging jets of 0.8 wt.-% CMC-7MF at $Cu_{j,gen} = 29{,}100$, $Re_{j,gen\text{-}BC} = 4770$ and $We_j = 1100$ is presented in Fig. 11(a). This atomization behavior was called the *open rim* pattern. A circular sheet with instability waves was observed near the impingement point. Downstream from the impingement point, the sheet was observed to form bow-shaped ligaments that were connected at the sheet centerline. The ligaments were observed to detach from the sheet and breakup into several drops, as presented in Fig. 12. Slightly increasing the inertial force to $Cu_{j,gen} = 32{,}600$, $Re_{j,gen\text{-}BC} = 5400$ and $We_j = 1380$ led to a small difference in the morphology of the spray. As presented in Fig. 11(b), the liquid structures appeared to be more unstable and were observed to breakup into bow shaped liga-

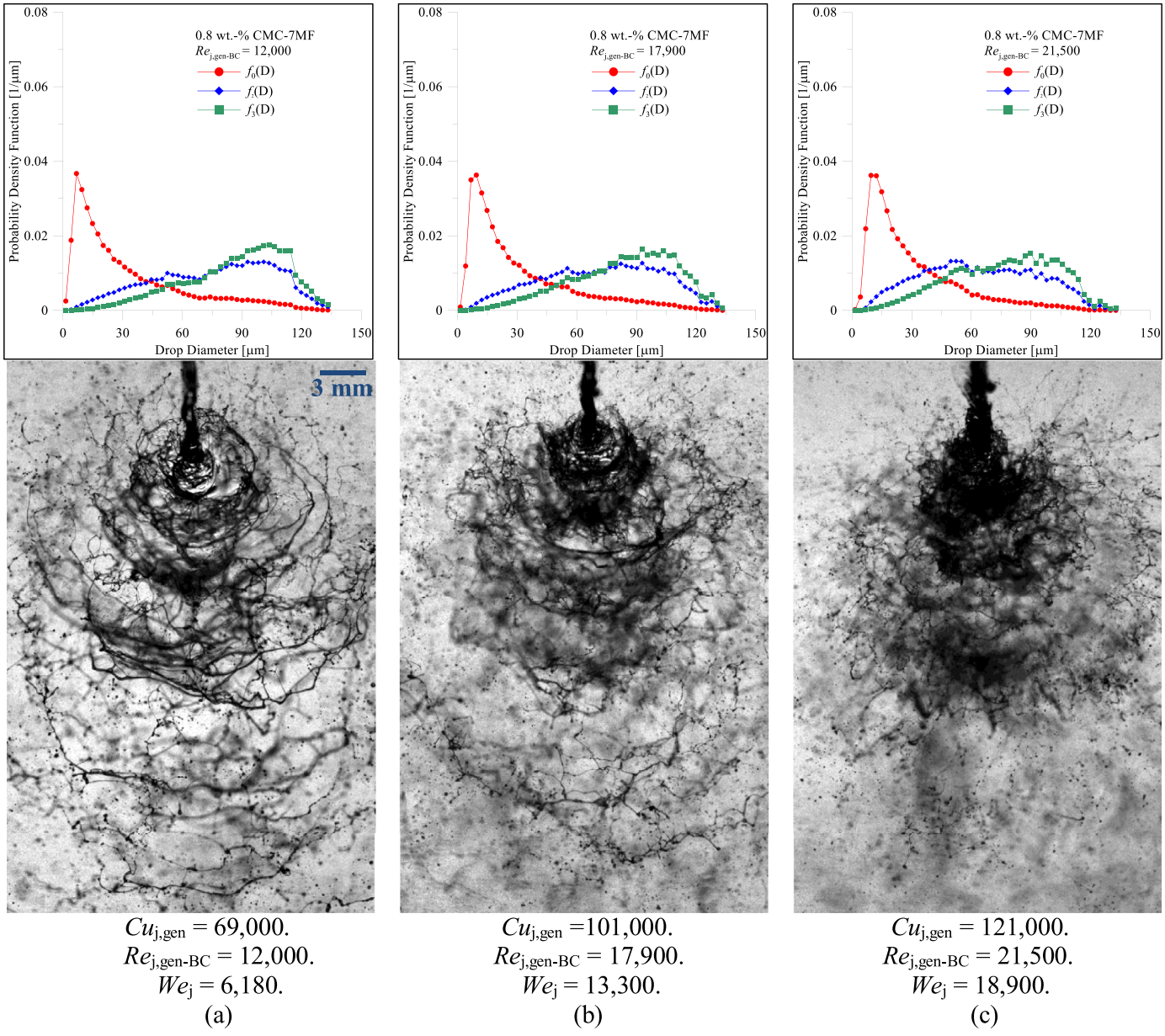

Fig. 13. Number, surface area, and volume pdfs versus drop diameters with corresponding spray patterns for select 0.8 wt.-% CMC-7MF sprays with increasing $Cu_{j,gen}$, $Re_{j,gen-BC}$, and We_j.

ments, which then experienced breakup into drops. Further increasing the inertial force to $Cu_{j,gen} = 46{,}100$, $Re_{j,gen-BC} = 7810$ and $We_j = 2760$, as presented in Fig. 11(c), led to the formation of a ligament web with various three-dimensional morphologies This atomization behavior was called the *ligament web* pattern. Similar to the 0.5 wt.-% CMC-7HF spray at relatively higher inertial forces ($Cu_{j,gen} \geq 361{,}100$, $Re_{j,gen-BC} \geq 12{,}600$, $We_j \geq 16{,}300$), it was difficult to determine where the liquid sheet experienced breakup and where the ligament web began. Ligaments were also observed to separate from the web further downstream and eventually drops were formed from the ligaments at these test conditions.

As presented in Fig. 11(d) for 0.8 wt.-% CMC-7MF at $Cu_{j,gen} = 69{,}000$, $Re_{j,gen-BC} = 12{,}000$, and $We_j = 6180$, further increasing the inertial force resulted in an increase in the denseness of the ligament web, the quantity of ligaments separating from the web, and the quantity of drops formed. A transition from the *ligament web* pattern to the *fully developed* pattern in observed by further increasing the inertial force. This transitioning to the fully developed pattern can be seen as early as Fig. 11(e) at $Cu_{j,gen} = 87{,}800$, $Re_{j,gen-BC} = 15{,}400$, and $We_j = 10{,}000$, before becoming even more pronounced with increasing inertial force from Fig. 11(f)–(h). The breakup process for the fully developed pattern is essentially that of the mechanism proposed by Dombrowski and Johns (1963). Impact waves originating from the impingement point travel downstream and lead to the formation of ligaments and eventually drops. Viscosity, which dampens out external perturbations, tends to move the maximum growth rate to higher wave numbers, which ultimately results in the formation of larger drops.

For the 0.8 wt.-% CMC-7MF liquid at conditions $Cu_{j,gen} \geq 69{,}000$, $Re_{j,gen-BC} \geq 12{,}000$, and $We_j \geq 6180$, Phase Doppler Anemometry also was used to measure the drop size at the centerline of the spray and at 5 cm below the impingement point. Fig. 13(a)–(c) presents the far-field spray patterns and the corresponding number probability density function f_0, surface area probability density function f_2, and volume probability density function f_3 for select

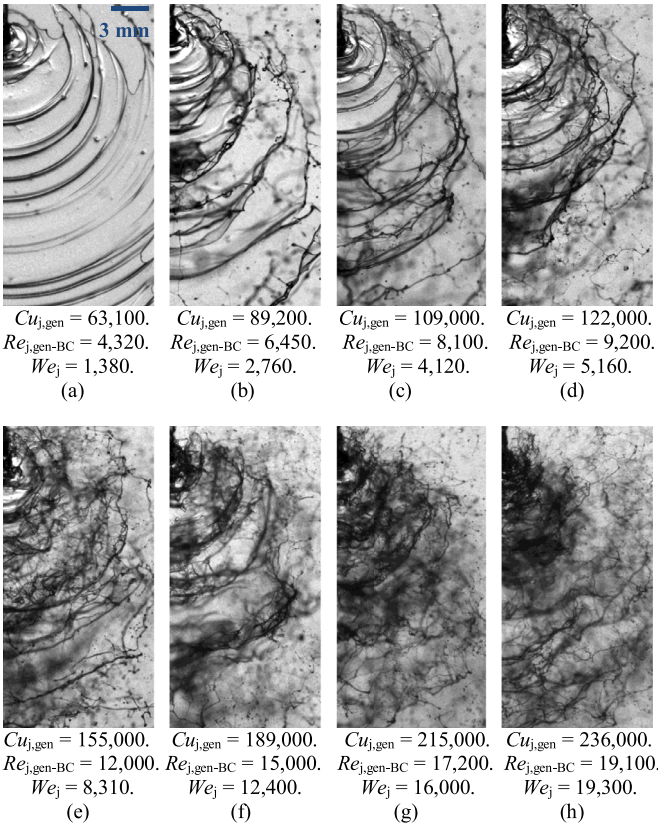

Fig. 14. Spray formation of 1.4 wt.-% CMC-7MF with increasing $Cu_{j,gen}$, $Re_{j,gen-BC}$, and We_j.

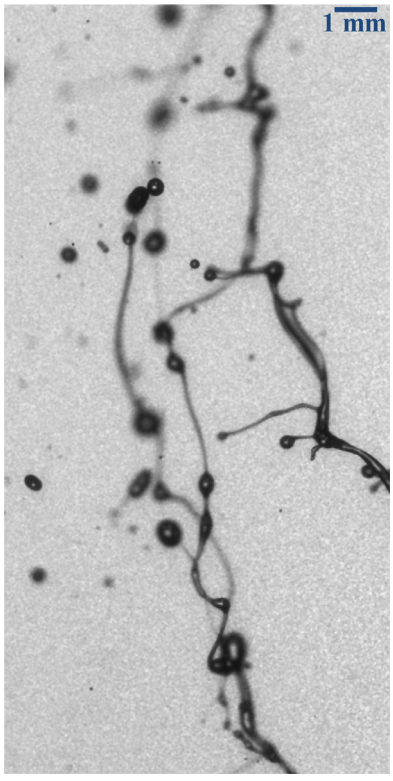

Fig. 15. Drop formation for 1.4 wt.-% CMC-7MF at $Cu_{j,gen} = 63{,}100$, $Re_{j,gen-BC} = 4320$, and $We_j = 1380$.

conditions. The pdfs were once again created using a bin size of 50 and a sample size of 50,000 drops at each test condition. The pdfs were not observed to vary significantly and indicated a high quality of atomization for the 0.8 wt.-% CMC-7MF spray at all test conditions considered.

The spray formation of two impinging jets of 1.4 wt.-% CMC-7MF at $Cu_{j,gen} = 63{,}100$, $Re_{j,gen-BC} = 4320$, and $We_j = 1380$ was observed to be that of a distinct ruffled circular sheet, as presented in Fig. 14(a). This atomization behavior was called the *ruffled sheet* pattern. Instabilities were once again observed on the sheet. However, instead of perforations, long ligaments that maintained connectivity with parts of the liquid sheet were observed. The ligaments then experienced breakup into a few large drops, as seen in Fig. 15. Increasing the inertial force to $Cu_{j,gen} = 89{,}200$, $Re_{j,gen-BC} = 6450$, and $We_j = 2760$ drastically changed the spray formation pattern. As presented in Fig. 14(b), a ligament web with various three-dimensional morphologies was observed. This atomization behavior was called the *perforated sheet* pattern. It was again difficult to differentiate between the regions of liquid sheet breakup and ligament formation. The ligaments were observed to separate from the web further downstream and drops were eventually formed from the ligaments. Interestingly, this spray pattern was similar to that of the 0.8 wt.-% CMC-7MF spray at $Cu_{j,gen} = 46{,}100$, $Re_{j,gen-BC} = 7810$, and $We_j = 2760$, as presented in Fig. 11(c). This is noteworthy because although two different concentrations of polymers were used for the liquid formulation, the generalized Bird–Carreau jet Reynolds number satisfactorily accounted for atomization behavior, and polymer concentration itself does not appear to be a discriminating factor.

Fig. 14(c) shows the spray pattern of 1.4 wt.-% CMC-7MF at $Cu_{j,gen} = 109{,}000$, $Re_{j,gen-BC} = 8100$, and $We_j = 4120$ transitioning from the *perforated sheet* pattern to the *ligament web* pattern. Further increasing the inertial force resulted in an increase in: the denseness of the ligament web, the quantity of ligaments separating from the web, and the quantity of drops formed. As presented in Fig. 14(d)–(h), the spray formation behavior transitioned from the *ligament web* pattern to the *fully developed* pattern with increasing inertial force. It should also be noted that these are common characteristics for some of the spray patterns for the 0.5 wt.-% CMC-7HF impinging jets, but their particular spray patterns were observed to be somewhat different. This difference is believed to be due to CMC-7HF possessing a higher molecular weight (700 kDa) compared to the molecular weight of CMC-7MF (250 kDa).

PDA was also used to measure the drop size and drop velocity of the 1.4 wt.-% CMC-7MF spray at conditions of $Cu_{j,gen} \geq 122{,}000$, $Re_{j,gen-BC} \geq 9200$, and $We_j \geq 5160$. Measurements were obtained at 5 cm below the impingement point at the centerline of the spray. Fig. 16(a)–(c) presents the far-field spray patterns and the corresponding number probability density function f_0, surface area probability density function f_2, and volume probability density function f_3 for select conditions and each pdf was created using a bin size of 50 and a sample size of 50,000 drops. No significant variation was observed in the number pdfs but the area and volume pdfs showed a decrease in probability density for relatively larger drops (>105 μm) and an increase in the probability density of mid-sized drops (between 45 μm and 105 μm) with increasing inertial force.

3.2. Intact sheet length

The fragmentation of bulk liquid to drops involves the breakup of the liquid sheet into ligaments, and the sheet breakup length serves as an indicator of the dynamics that govern the eventual drop size. A clear *sheet breakup length* was difficult to define for some of the breakup modes observed for the three non-Newtonian

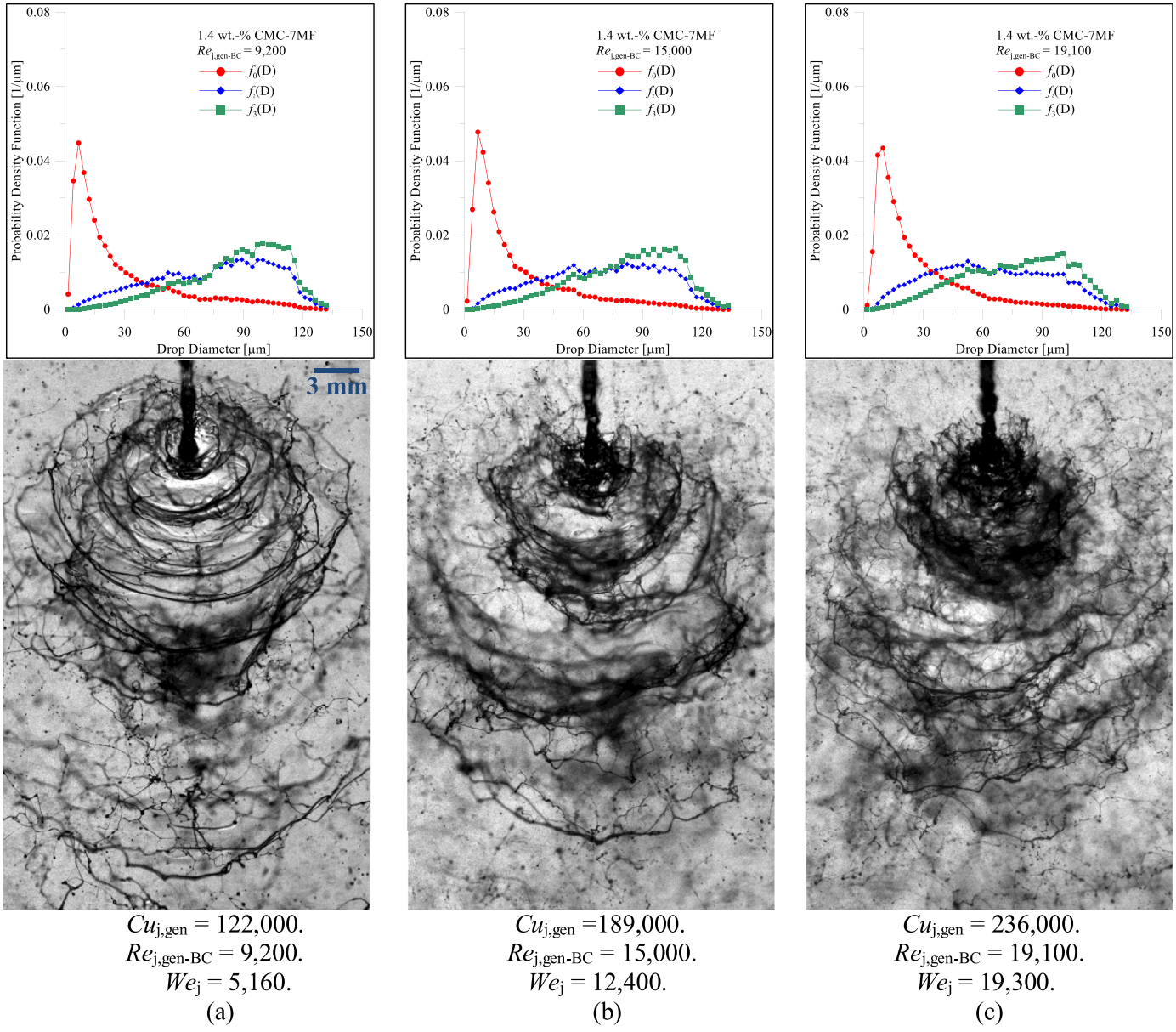

Fig. 16. Number, surface area, and volume pdfs versus drop diameters with corresponding spray patterns for select 1.4 wt.-% CMC-7MF sprays with increasing $Cu_{j,gen}$, $Re_{j,gen-BC}$, and We_j.

liquids considered in this work. This was particularly the case for the *tangled web* and *ligament web* patterns since parts of the web-like structures were still attached to the liquid sheet. Therefore, an *intact sheet length* is used here in lieu of the sheet breakup length and is simply defined as the length from the impingement point to the point where the sheet is no longer intact. For the *ligament web* and the *tangled web* patterns, this would mean the length from the impingement point to the start of the web-like structure. For the *open rim, perforated sheet, ruffled sheet*, and *full developed sheet* the intact sheet length would be identical to the sheet breakup length – from the impingement point to the point where the sheet is no longer exists. It is thought that the same destructive aerodynamic forces on the liquid sheet that promote the sheet to disintegrate into ligaments in some modes, instead cause the liquid sheet to disintegrate into the web-like structure in other modes. Fig. 17 presents the dimensionless intact sheet length X_b as a function of the generalized Bird–Carreau jet Reynolds number $Re_{j,gen-BC}$. The intact sheet length was observed to decrease with increasing $Re_{j,gen-BC}$ due to the increased destructive inertial force resulting in greater instabilities on the liquid sheet. The trend of shorter intact sheet length with increasing inertial force is consistent with earlier observations in both Newtonian (Ryan et al., 1995) and non-Newtonian (Baek et al., 2011; Yang et al., 2012) literature. Since the intact sheet length of the three CMC liquids appear to collapse onto a single curve as a function of $Re_{j,gen-BC}$, an empirical correlation for the dimensionless intact sheet length (made dimensionless using the orifice diameter) that depends only on the generalized Bird–Carreau jet Reynolds number is:

$$\frac{X_b}{d_0} = 3.368\left(0.0001 Re_{j.gen-BC}\right). \tag{8}$$

Ryan et al. (1995) provides an analytical expression for the sheet breakup length using an inviscid instability analysis of a liquid sheet:

$$\frac{X_b}{d_0} = 5.451\left(\frac{\rho_g}{\rho_L}\right)^{-2/3}\left(We_j \frac{(1-\cos\theta)^2}{\sin^3\theta}\right)^{-1/3} \tag{9}$$

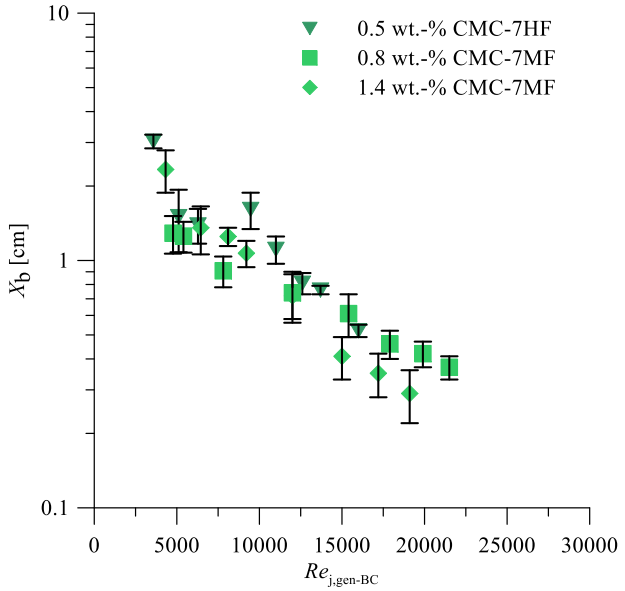

Fig. 17. Intact sheet length X_b vs. the generalized Bird-Carreau jet Reynolds number $Re_{j,gen\text{-}BC}$.

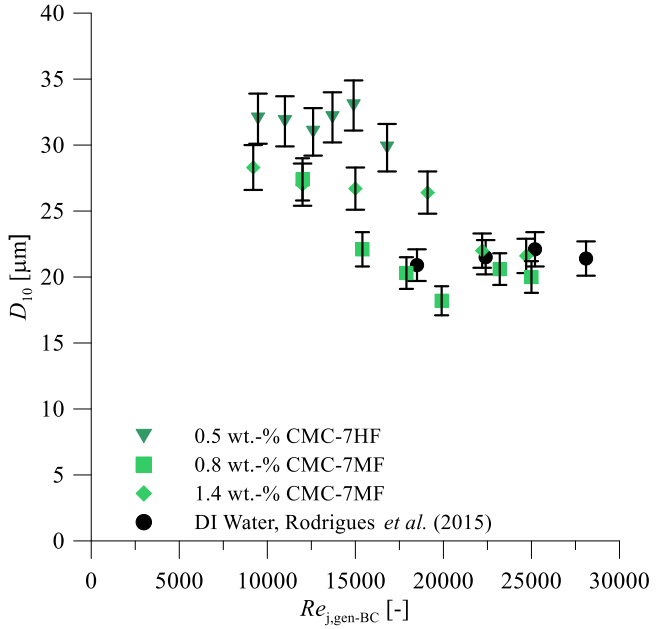

Fig. 19. D_{10} as function of $Re_{j,gen\text{-}BC}$ for three CMC liquids and water.

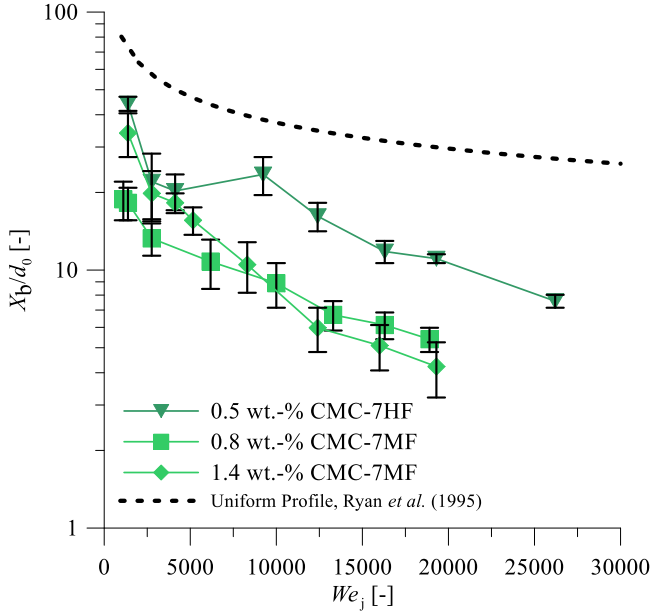

Fig. 18. Experimental and predicted dimensionless intact sheet length X_b/d_0 vs. the jet Weber number We_j.

Fig. 18 presents a comparison, as a function of the jet Weber number, between the predicted sheet breakup length using the inviscid analysis of Ryan et al. (1995) and the experimental intact sheet length for the three CMC solutions used in this work. Based on Fig. 18, it can be inferred that the liquid viscosity influences the intact sheet length. The sprays formed by CMC-7HF possessed the highest effective jet liquid viscosity (as presented in Fig. 6) and were also found to possess a larger intact sheet length compared to the two CMC-7MF solutions at similar jet Weber numbers. Although the Ryan et al. (1995) model agrees with the experimental results in trend, it actually over-predicts the intact sheet length at the range of jet Weber numbers considered. The inviscid instability analysis only qualitatively agreeing with, but quantitatively over-predicting experimental results in the higher Weber number regimes has been noted in previous works in literature such as the same Ryan et al. (1995) study, Anderson et al. (2006) and Rodrigues et al. (2015). One would expect that the influence of viscous effects would lead to larger experimental intact sheet lengths compared to those predicted by the inviscid model. However, it is a deficiency in the inviscid model itself that leads to over-predictions of the intact sheet length for inviscid liquids, as well as for the viscous non-Newtonian liquids used in this work. It is not believed that the model over-prediction is due to the different definitions of sheet length (sheet breakup length versus intact sheet length), since both definitions incorporate the destructive aerodynamic forces on the liquid sheet promoting sheet disintegration.

3.3. Droplet diameter

The arithmetic mean diameter, Sauter mean diameter, and Mass Median Diameter were computed based on the PDA measurements. The arithmetic mean diameter D_{10} versus generalized Bird–Carreau jet Reynolds number $Re_{j,gen\text{-}BC}$ for the three CMC solutions is presented in Fig. 19. The measured D_{10} drop diameters of the 0.5 wt.-% CMC-7HF spray were not observed to vary significantly with increasing $Re_{j,gen\text{-}BC}$ and remained at approximately 30 μm, indicating a similar plateau. The D_{10} mean drop diameter for the 0.8 wt.-% CMC-7MF and 1.4 wt.-% CMC-7MF sprays were observed to decrease from about 27 μm to 20 μm with increasing inertial force through the generalized Bird–Carreau jet Reynolds number. PDA measurements of DI water previously reported by Rodrigues et al. (2015), which are also included in Fig. 19 for the sake of reference, were previously observed to remain relatively constant at ~21 μm over a range of $6820 \leq We_j \leq 21{,}900$ (corresponding to $18{,}400 \leq Re_{j,gen\text{-}BC} \leq 33{,}100$). Recall that for a Newtonian liquid, η_0 and η_∞ are both equal to the Newtonian dynamic viscosity and the flow behavior index $n = 1$. The constant D_{10} water measurements over this range were believed to be due to the fine level of atomization at the considered high Weber number operating regime (Rodrigues et al., 2015). A few of the measured D_{10} diameters for the 0.8 wt.-% CMC-7MF spray was actually lower than the D_{10} of the DI water spray at a similar $Re_{j,gen\text{-}BC}$. However, it should be noted that even though $Re_{j,gen\text{-}BC}$ were of similar values for such test conditions, the jet Weber number of the CMC sprays

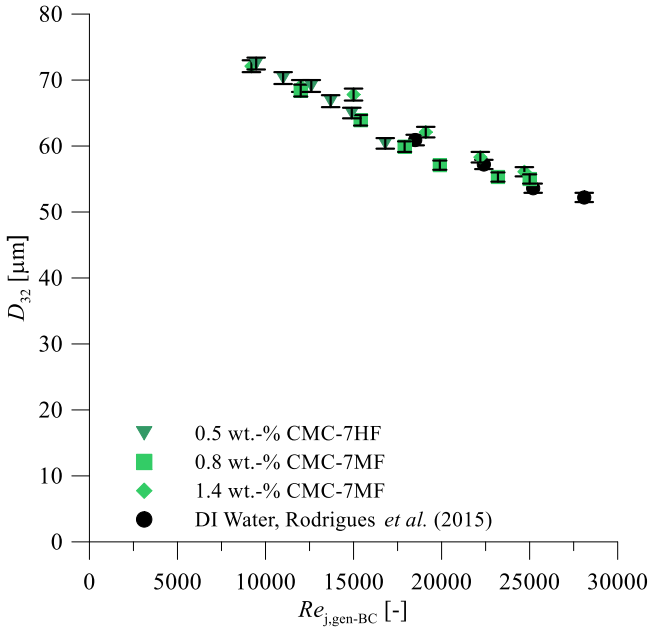

Fig. 20. D_{32} as function of $Re_{j,gen\text{-}BC}$ for three CMC liquids and water.

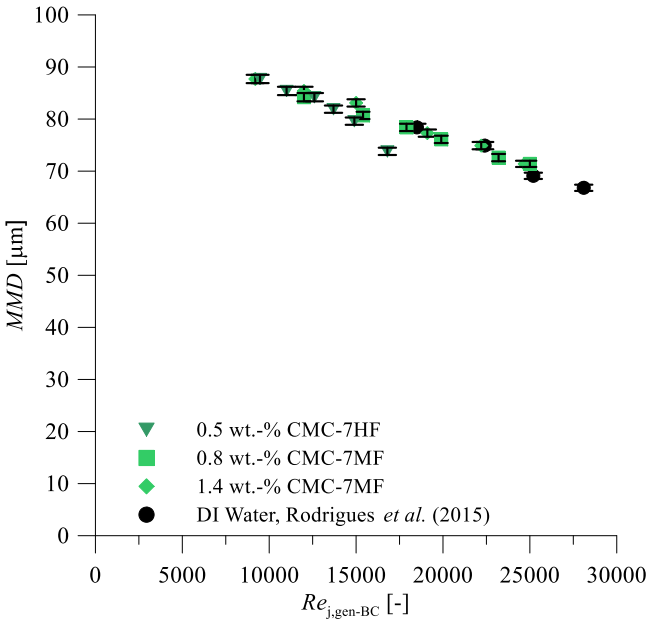

Fig. 21. *MMD* as function of $Re_{j,gen\text{-}BC}$ for three CMC liquids and water.

were actually much larger than those of the DI water sprays (since the CMC sprays possessed a viscosity greater than the DI water sprays).

Both the D_{32} and *MMD* values of all three CMC liquids were observed to decrease with increasing generalized Bird–Carreau jet Reynolds number, as presented in Figs. 20 and 21 respectively. The decrease in these two mean diameters is due to the increase in the destructive inertial force over the stabilizing viscous force for greater $Re_{j,gen\text{-}BC}$. Interestingly, measurements for all three CMC liquids and DI water sprays seemed to follow a single curve for both of these mean drop diameters. Furthermore, D_{32} and *MMD* values do not appear to be affected by transitions in the atomization regimes. Rather, as the generalized Bird–Carreau jet Reynolds number is increased, fewer and fewer of the largest diameters were observed to be present in the spray.

Empirical correlations for dimensionless D_{32} and *MMD* that depends only on the generalized Bird–Carreau jet Reynolds number are:

$$\frac{D_{32}}{d_0} = \frac{1.83}{(Re_{j,gen-BC})^{0.309}}, \tag{10}$$

$$\frac{MMD}{d_0} = \frac{1.21}{(Re_{j,gen-BC})^{0.242}}. \tag{11}$$

D_{32} and *MMD* were made dimensionless using the orifice diameter d_0. The single curve observed for D_{32} and *MMD* measurements show the relevance of $Re_{j,gen\text{-}BC}$ as a valid parameter for presenting spray characteristics of non-Newtonian impinging jet sprays, particularly when elastic, thixotropic, and molecular structure differences are insignificant. A strong variation in D_{32} and *MMD* compared to D_{10} seems to indicate that the relatively smaller drops are formed in roughly the same amounts regardless of the generalized Bird–Carreau jet Reynolds number but the larger drops begin to disappear from the spray with greater $Re_{j,gen\text{-}BC}$.

Ryan et al. (1995) also provides a closed form analytical expression for drop diameter d_D, which is derived from the earlier work in linear instability of a liquid sheet by Dombrowski and Johns (1963). The expression for predicted drop diameter provided by Ryan et al. is:

$$\frac{d_D}{d_0} = 1.144\left(\frac{\rho_g}{\rho_L}\right)^{-1/6}\left(We_j\frac{(1-\cos\theta)^2}{\sin^3\theta}\right)^{-1/3} \tag{12}$$

Anderson et al. (2006) and Rodrigues et al. (2015) noted, however, that although the instability model agrees in trend, it consistently over-predicts drop diameter in the high Weber number regime. Rodrigues et al. (2015) presented an analytical expression for drop diameter that incorporates the jet velocity profile, based upon the work of Bremond and Villermaux (2006) and Choo and Kang (2007). This expression for drop diameter presented by Rodrigues et al. (2015) is:

$$\frac{d_D}{d_0} = 1.144\left(\frac{\rho_g}{\rho_L}\right)^{-1/6}\left(We_j\frac{(1-\cos\theta)^2}{\sin^3\theta}\right)^{-1/3}\frac{d_D}{d_0} = \frac{1.14(K*)^{1/3}}{\alpha^{2/3}s^{2/3}We_j^{1/3}}. \tag{13}$$

In the above equation, K^* is the dimensionless sheet thickness parameter, and α is the ratio of sheet velocity to jet velocity.

Although there have been some efforts to incorporate non-Newtonian viscous effects into analytical instability models, such as Mallory and Sojka (2014b), no closed form analytical model currently exists in literature. Therefore, the inviscid model of Ryan et al. (1995) and the inviscid model of Rodrigues et al. (2015), with the parabolic profile assumption, will be used in this work to compare experimental D_{32} and *MMD* of the three CMC liquids sprays with predicted diameters. The inviscid model does not seem unreasonable for an initial comparison to the experimental data due to the high generalized jet Carreau numbers considered, which resulted in the apparent viscosity within the orifice to be within an order of magnitude to that of water. Fig. 22(a) and (b) presents the dimensionless D_{32}/d_0 and MMD/d_0 respectively as a function of the jet Weber number. Similar to the intact sheet length comparison, the Ryan et al. (1995) model over-predicts the drop diameters. On the other hand, decent agreement is observed using the Rodrigues et al. (2015) model with the parabolic profile assumption.

3.4. Drop velocity

The mean axial drop velocity $U_{z\text{-mean}}$ was observed to increase for greater generalized BC jet Reynolds numbers $Re_{j,gen\text{-}BC}$ for all

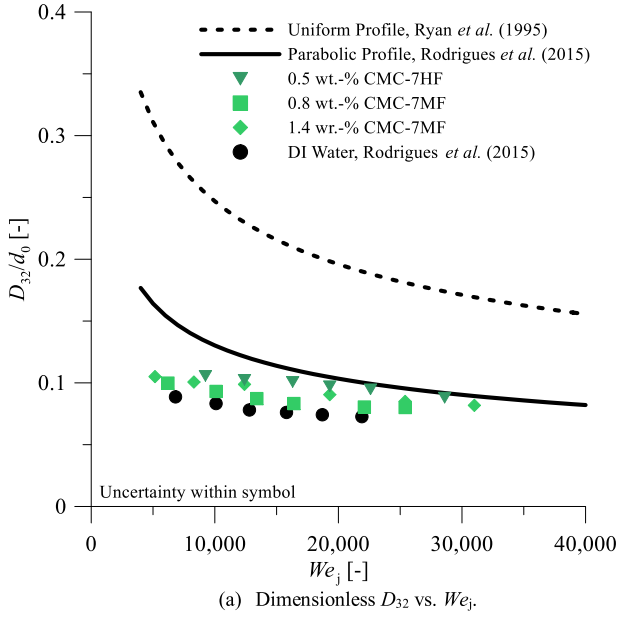

(a) Dimensionless D_{32} vs. We_j.

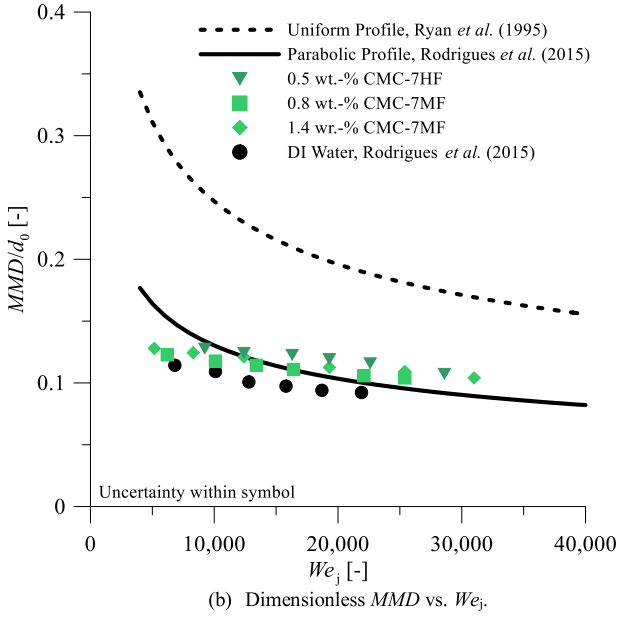

(b) Dimensionless *MMD* vs. We_j.

Fig. 22. Dimensionless D_{32} and *MMD* with predicted drop diameters vs. jet Weber number We_j.

three CMC liquids. This can be attributed to the increase in the inertial force through the mean jet velocity. Fig. 23 presents the mean axial drop velocity vs. $Re_{j,gen\text{-}BC}$ for the three CMC liquids along with measurements of water from Rodrigues et al. (2015) as reference. Note that the vertical bars in Fig. 23 represent the root-mean square (RMS) of velocity and not the measurement uncertainty; the measurement uncertainty of 2.9% is contained within the symbol itself.

A more detailed look at the axial drop velocity with the aid of the velocity probability density function would be useful due to the rather large axial drop velocity RMS. A bin size of 50 was again used to produce the velocity pdfs. Fig. 24(a)–(c) presents the velocity pdf for the 0.5 wt.-% CMC-7HF, 0.8 wt.-% CMC-7MF, and 1.4 wt.-% sprays. The mean drop velocity was made dimensionless using the mean axial drop velocity in order to provide a more relative comparison. For each of these liquids, increasing $Re_{j,gen\text{-}BC}$ decreased the peak of the drop velocity with the greatest probability density. In other words, the drop velocities in the spray were observed to become more polydisperse with increasing $Re_{j,gen\text{-}BC}$ due to the greater inertial force. This is consistent with the observation for velocity pdfs of water sprays by Rodrigues et al. (2015).

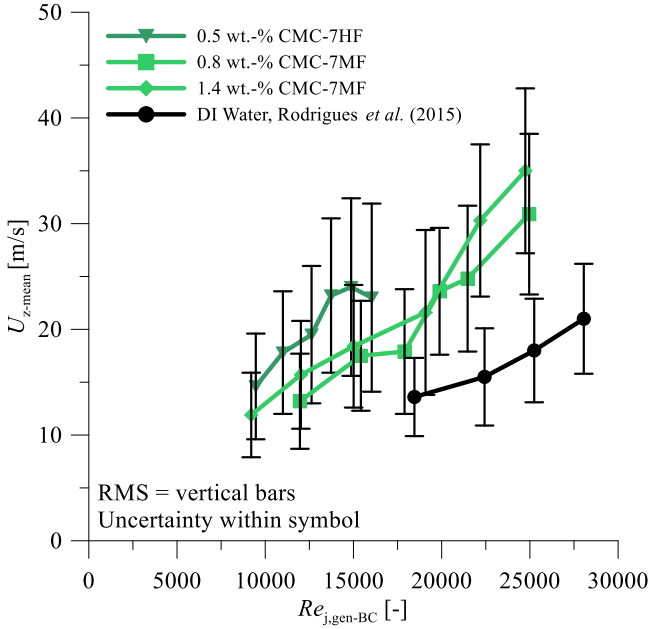

Fig. 23. Mean axial drop velocity $U_{z\text{-}mean}$ as function of $Re_{j,gen\text{-}BC}$ for three CMC liquids and water.

4. Summary and conclusions

The spray formation and spray characteristics of three viscous, non-Newtonian liquids (0.5 wt.-% CMC-7HF, 0.8 wt.-% CMC-7MF, and 1.4 wt.-% CMC-7MF) were experimentally studied in this work. The Bird–Carreau rheological model was used to describe the shear-thinning behavior of the liquids used. A jet Carreau number Cu_j, generalized Bird–Carreau jet Reynolds number $Re_{j,gen\text{-}BC}$, and jet Weber number We_j were used as the primary parameters to characterize the impinging jet sprays. Incorporating the use of dimensionless numbers to characterize the sprays produced by the propellant simulants considered in this work allows for the observations revealed here to be used in the design of rocket combustion chambers for real propellants.

Shadowgraphs showed the transition in the spray patterns as a function of the generalized jet Carreau number $Cu_{j,gen\text{-}BC}$, generalized BC jet Reynolds number $Re_{j,gen\text{-}BC}$, and the jet Weber number We_j. Several spray patterns were observed including: perforated sheet, tangled web, and ligament web for the 0.5 wt.-% CMC-7HF; open rim, ligament web, and fully developed for the 0.8 wt.-% CMC-7HF; ruffled sheet, perforated sheet, ligament web, and fully developed for the 1.4 wt.-% CMC-7MF spray. Future work with respect to the spray patterns observed in this study includes determining why the presence of the web-like structures were more prevalent in the 0.5 wt.-% CMC-7MF sprays compared to the 0.8 wt.-% CMC-7MF and 1.4 wt.-% CMC-7MF sprays. In particular, characterization of the rheology for the three liquids in an elongational flow may yield further insight on the flow physics behind the formation and prevalence of the web-like structures for a given liquid at a particular test condition.

The intact sheet length was extracted from the shadowgraphs and was observed to follow a single curve as a function of $Re_{j,gen\text{-}BC}$. A PDA system was used to measure the drop size and drop velocity and characteristic drop sizes of D_{10}, D_{32}, and MMD

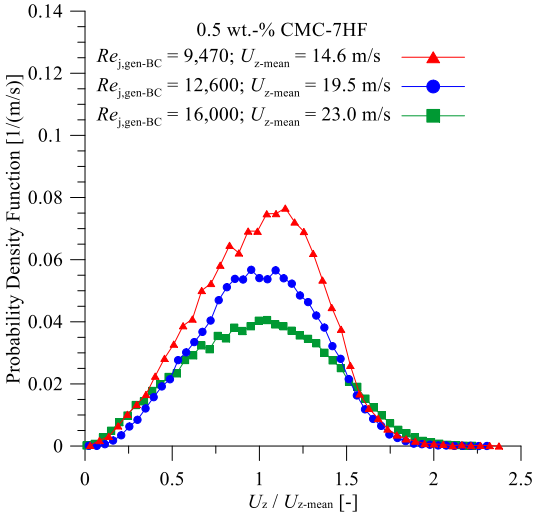

(a) Velocity pdf for 0.5 wt.-% CMC-7HF.

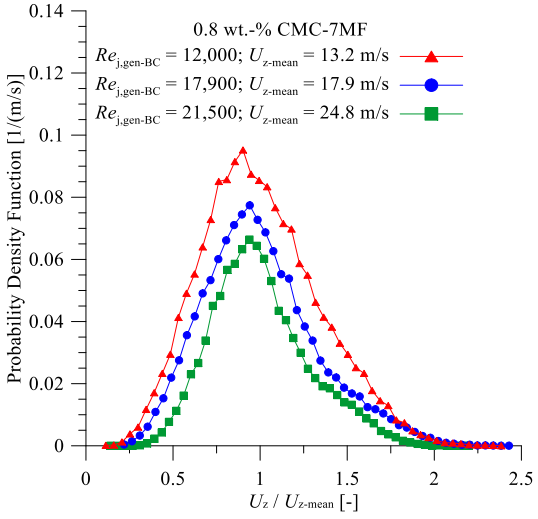

(b) Velocity pdf for 0.8 wt.-% CMC-7MF.

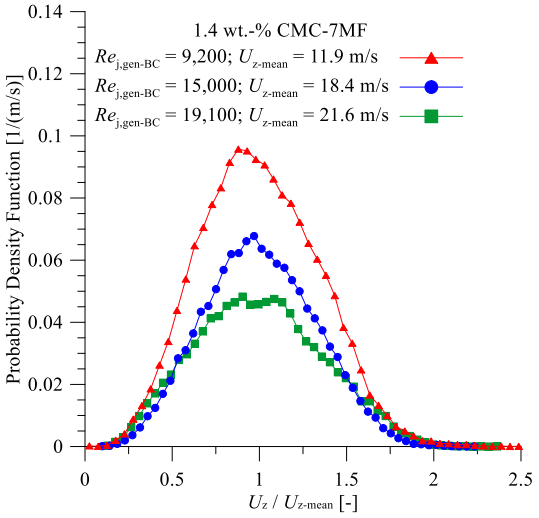

(c) Velocity pdf for 1.4 wt.-% CMC-7MF.

Fig 24. Axial drop velocity pdf vs. normalized axial drop velocity for three CMC liquids at select test conditions.

and the mean axial drop velocity $U_{z\text{-mean}}$ with its root-mean square were reported along with pdfs for diameter and velocity. D_{32} and *MMD* were also observed to each follow a single curve depending on $Re_{j,gen-BC}$. The intact sheet length, D_{32}, and *MMD* each collapsing onto a single curve seems to indicate that the results obtained for the propellant simulants in this work can be scaled by design of rocket combustion chambers to real propellants. Greater mean axial drop velocities were observed with increasing $Re_{j,gen-BC}$. Intact sheet length closer to the impingement point, smaller drop sizes, and greater mean axial drop velocities were all observed with increasing $Re_{j,BC-gen}$, and these can be attributed to the increased inertial force over the viscous force. Although a closed-form analytical model that accounts for viscous non-Newtonian behavior remains an open problem in the literature, the measurements presented in this work could be used to validate a future model.

Acknowledgments

The research presented in this paper was made possible with the financial support of the U.S. Army Research Office under the Multi-University Research Initiative grant number W911NF-08-1-0171. The authors wish to thank Prof. Jennifer Mallory for helpful feedback, Dr. Ariel Muliadi for assistance with PDA configuration, and Prof. Osvaldo Campanella for access to rheometers.

References

Albrecht, H.E., Borys, M., Damaschke, N., Tropea, C., 2003. Laser Doppler and Phase Doppler Measurement Techniques. Springer, Berlin, p. 2003.
Anderson, W.E., Ryan, H.M., Santoro, R.J., 2006. Impact wave-based model of impinging jet atomization. Atomization Sprays 16 (7), 791–805.
Baek, G., Kim, S., Han, J., Kim, C., 2011. Atomization characteristics of impinging jets of gel material containing nanoparticles. J. Non-Newtonian Fluid Mech 166, 1272–1285.
Bremond, N., Villermaux, E., 2006. Atomization by jet impact. J. Fluid Mech. 549, 273–306.
Carreau, P.J., 1972. Rheological equations from molecular network theories. Trans. Soc. Rheol. 16, 99–127.
Chojnacki, K.T., Feikema, D.A., 1997. Study of non-Newtonian liquid sheets formed by impinging jets. JPC 1997, 33rd Joint Propulsion Conference and Exhibit.
Choo, Y.J., Kang, B.S., 2007. The effect of jet velocity profile on the characteristics of thickness and velocity of the liquid sheet formed by two impinging jets. Phys. Fluids A: Fluid Dyn. 19, 101–107.
Dombrowski, N., Johns, W.R., 1963. The aerodynamic instability and disintegration of viscous liquid sheets. Chem. Eng. Sci. 18, 203–214.
Fakhri, S., Lee, J.G., Yetter, R.A., 2010. Effect of nozzle geometry on the atomization and spray characteristics of gelled-propellant simulants formed by two impinging jets. Atomization Sprays 20, 1033–1046.
Heidmann, M.F., Priem, R.J., Humphrey, J.C., 1957. A Study of the Sprays Formed by Two Impinging Jets. National Advisory Committee for Aeronautics Technical Note 3835.
Humble, R.W., Henry, G.N., Larson, W.J., 1992. Space Propulsion Analysis and Design. McGraw-Hill, New York.
Ibrahim, E.A., Przekwas, A.J., 1991. Impinging jet atomization. Phys. Fluids A: Fluid Dyn. 3, 2981–2987.
Kline, S.J., McClintock, F.A., 1953. Describing uncertainties in single sample experiments. Mech. Eng. 75, 3–8.
Lefebvre, A., 1989. Atomization and Sprays. Hemisphere, New York.
Li, R., Ashgriz, N., 2006. Characteristics of liquid sheets formed by two impinging jets. Phys. Fluids 18, 87–104.
Ma, Y.C., Bai, F.Q., Chang, Q., Yi, J.M., Jiao, K., Du, Q., 2015. An experimental study on the atomization characteristics of impinging jets of power law fluid. J. Non-Newtonian Fluid Mech. 217, 49–57.
Madlener, K., Ciezki, H.K., 2012. Estimation of flow properties of gelled fuels with regard to propulsion systems. J. Propul. Power 28, 113–121.
Mallory, J.A., Sojka, P.E., 2014a. On the primary atomization of non-Newtonian impinging jets: volume I experimental investigation. Atomization Sprays 24, 431–465.
Mallory, J.A., Sojka, P.E., 2014b. On the primary atomization of non-Newtonian impinging jets: volume II linear stability theory. Atomization Sprays 24, 525–554.
Morrison, F., 2001. Understanding Rheology. Oxford University Press, New York.
Nathan, B., Rahimi, S., 2002. The status of gel propellants in Year 2000. Int. J. Energetic Mater. Chem. Propulsion 5, 172–194.
Negri, M., Ciezki, H.K., Schlechtriem, S., 2013. Spray behavior of non-Newtonian fluids: correlation between rheological measurements and droplets/threads formation. Prog. Propul. Phys. 4, 271–290.
Palaszewski, B., 1994. Lunar missions using advanced chemical propulsion: system design issues. J. Spacecraft Rockets 31, 458–465.

Rodrigues, N.S., 2014. Impinging Jet Spray Formation Using Non-Newtonian Liquids M.S. thesis. School of Mechanical Engineering, Purdue University, West Lafayette.
Rodrigues, N.S., Kulkarni, V., Gao, J., Chen, J., Sojka, P.E., 2015. An experimental and theoretical investigation of spray characteristics of impinging jets in impact wave regime. Exp. Fluids 56, 1–13.
Ryan, H.M., Anderson, W.E., Pal, S., Santoro, R.J., 1995. Atomization characteristics of impinging liquid jets. J. Propul. Power 11, 135–145.
Shenoy, A.V., 2013. Rheology of Filled Polymer Systems. Springer Science and Business Media, Pune, India.
Von Kampen, J., Ciezki, H.K., Tiedt, T., Madlener, K., 2006. Some aspects of the atomization behavior of Newtonian and of shear-thinning gelled non-Newtonian fluids with an impinging jet injector. JPC 2006, 42nd Joint Propulsion Conference and Exhibit.
Xiao, H., Shi, Y., Xu, Z., Kim, L., Li, D., Lyu, S., 2015. Atomization characteristics of gelled hypergolic propellant simulants. Int. J. Precis. Eng. Manuf. 16, 743–747.
Yang, L.J., Fu, Q.F., Qu, Y.Y., Gu, B., Zhang, M.Z., 2012. Breakup of a power-law liquid sheet formed by an impinging jet injector. Int. J. Multiphase Flow 39, 37–44.
Zuidema, H., Waters, G., 1941. Ring method for determination of interfacial tension. Ind. Eng. Chem. 13, 312–313.